# Kinematics of the local universe : XII. 21-cm line measurements of 586 galaxies with the new Nançay receiver

Gilles Theureau, N. Coudreau, N. Halle, M. Hanski, L. Alsac, L. Bottinelli, L. Gouguenheim, J.-M. Martin, G. Paturel

A&A 430, 373–383 (2005)
DOI: 10.1051/0004-6361:20047152


Astronomy & Astrophysics

# Kinematics of the local universe

## XII. 21-cm line measurements of 586 galaxies with the new Nançay receiver⋆

G. Theureau[1,2], N. Coudreau[1], N. Hallet[1], M. Hanski[2,3], L. Alsac[4], L. Bottinelli[1], L. Gouguenheim[1], J.-M. Martin[1], and G. Paturel[5]

[1] Observatoire de Paris/Meudon, GEPI/CNRS URA1757, 92195 Meudon Principal Cedex, France
e-mail: theureau@obspm.fr
[2] LPCE/CNRS UMR6115, 45071 Orléans Cedex 02, France
[3] Tuorla Observatory, 21500 Piikkiö, Finland
[4] Sation de Radioastronomie, 18330 Nançay, France
[5] Observatoire de Lyon, 69561 Saint-Genis Laval Cedex, France

Received 27 January 2004 / Accepted 16 August 2004

**Abstract.** This paper presents 586 new 21-cm neutral hydrogen line measurements carried out with the FORT receiver of the meridian transit Nançay radiotelescope in the period July 2000−March 2003. This observational programme is part of a larger project aiming at collecting an exhaustive and magnitude-complete HI extragalactic catalogue for Tully-Fisher applications. It is associated with the building of the MIGALE spectroscopic archive and database.

**Key words.** astronomical data bases: miscellaneous – surveys – galaxies: kinematics and dynamics – radio lines: galaxies

## 1. Introduction

The present paper complements the KLUN[1] data-series (I: Bottinelli et al. 1992; II: Bottinelli et al. 1993; III: di Nella et al. 1996, VII: Theureau et al. 1998) with a collection of HI line measurements acquired with the new Nançay radiotelescope receiver (FORT). This programme has received the label of key project of the instrument and is allocated on average 20% of observing time since the first light in mid 2000.

The input catalogue has been carried out from a compilation of the HYPERLEDA extragalactic database completed by the 2.7 million galaxy catalogue extracted from the DSS (Paturel et al. 2000), and the successive releases of DENIS (DEep Near Infrared Survey, Mamon et al. 2004) and 2MASS (2 Micron All Sky Survey, Jarret et al. 2000) near infrared CCD surveys. The aim of the programme is to build a large all sky sample of spiral galaxies, complete down to well defined magnitude limits in the five photometric bands $B$, $I$, $J$, $H$ and $K$, and to allow peculiar velocity mapping of galaxies up to 10 000 km s$^{-1}$ in radial velocity, i.e. up to a scale greater than the largest structures of the Local Universe (Hanski 2003). This programme is unique and complementary to other HI projects such as HIPASS in Parkes (Barnes et al. 2001) which is very shallow and restricted to the very close universe or the future ALFA-project in ARECIBO[2] which will cover only a small portion of the sky for the deepest survey. It also complements the Fundamental Plane surveys (6dF[3], Jones et al. 2004, FP200[4] survey, Hudson et al. 2004) already in progress which are mainly concerned with cluster galaxies and shorter scales (see e.g. Mamon 2000; or Willick 2000). This kind of data is crucial for mapping the total mass distribution and for providing strong constraints on cosmological models and large scale structure formation.

From our 586 HI detections, we extract a high quality subsample of 368 21-cm line profiles suitable for a Tully-Fisher analysis. Adding these to our last general compilation presented in Paturel et al. (2003), we obtain a catalogue of more than 17 200 galaxies having an HI line measurement in the MIGALE/HYPERLEDA database[5].

The paper is structured as follows: the Nançay radiotelescope and processing chain are briefly presented in Sect. 2. The

⋆ Tables 2, 3 and HI-profiles and corresponding comments are only available in electronic form at the CDS via anonymous ftp to cdsarc.u-strasbg.fr (130.79.128.5) or via http://cdsweb.u-strasbg.fr/cgi-bin/qcat?J/A+A/430/373, or directly at our web site http://klun.obs-nancay.fr

[1] for Kinematics in the Local UNiverse.

[2] http://alfa.naic.edu/

[3] http://www.mso.anu.edu.au/6dFGS/

[4] http://astro.uwaterloo.ca/ mjhudson/fp200

[5] Multiparametric virtual instrument to study galaxy evolution; http://www-obs.univ-lyon1.fr/hypercat/ and http://www.cai-mama.obspm.fr/migale/

**Table 1.** Template radio sources; Col. 1: source index; Col. 2: source name; Col. 3: reference for flux measurement; Col. 4: reference flux at 1380 MHz; Col. 5: reference flux at 1420 MHz; Col. 6: object type from Veron et al. (1972) or Kuhr et al. (1981).

| | Name | Ref. | 1380 MHz | 1410 MHz | Object type |
|---|---|---|---|---|---|
| 1 | 0023-26 | Kuhr et al. (1981) | 8.84 | 8.71 | |
| 2 | 0134+32 3C 48 | Baars et al. (1977) | 16.12 | 15.85 | quasi-stellar source |
| 3 | 0237-23 | Kuhr et al. (1981) | 6.58 | 6.55 | quasi-stellar source |
| 4 | 0316+16 CTA 21 | Kuhr et al. (1981) | 8.18 | 8.09 | "empty field" |
| 5 | 0356+10 3C 98 | Kuhr et al. (1981) | 12.00 | 11.82 | galaxy |
| 6 | 0433+29 3C 123 | Baars et al. (1977) | 49.23 | 48.41 | galaxy |
| 7 | 0710+11 3C 175 | Witzel et al. (1970) | 2.59 | 2.543 | quasi-stellar source |
| 8 | 0809+48 3C 196 | Witzel et al. (1970) | 14.32 | 14.08 | quasi-stellar source |
| 9 | 0915-11 3C 218 | Baars et al. (1977) | 43.62 | 42.78 | galaxy |
| 10 | 1005+07 3C 237 | Kuhr et al. (1981) | 6.86 | 6.731 | "empty field" |
| 11 | 1040+12 3C 245 | Kuhr et al. (1981) | 3.27 | 3.23 | quasi-stellar source |
| 12 | 1127-14 | Gardner et al. (1975) | 6.78 | 6.76 | quasi-stellar source |
| 13 | 1151-34 | Kuhr et al. (1981) | 6.68 | 6.04 | quasi-stellar source |
| 14 | 1245-19 | Kuhr et al. (1981) | 5.60 | 5.54 | |
| 15 | 1328+30 3C 286 | Baars et al. (1977) | 14.94 | 14.78 | quasi-stellar source |
| 16 | 1409+52 3C 295 | Baars et al. (1977) | 22.60 | 22.20 | galaxy |
| 17 | 1425-01 3C 300.1 | Witzel et al. (1970) | 2.93 | 2.89 | "empty field" |
| 18 | 1514+07 3C 317 | Witzel et al. (1970) | 5.50 | 5.38 | galaxy |
| 19 | 1602-28 | Gardner et al. (1975) | 2.85 | 2.77 | |
| 20 | 1641+39 3C 345 | Witzel et al. (1970) | 6.80 | 6.77 | quasi-stellar source |
| 21 | 2117+60 3C 430 | Witzel et al. (1970) | 7.56 | 7.44 | galaxy |
| 22 | 2203-18 | Gardner et al. (1975) | 6.74 | 6.68 | quasi-stellar source |
| 23 | 2314+03 3C 459 | Kuhr et al. (1981) | 4.64 | 4.54 | galaxy |

characteristics of the input catalogue are listed in Sect. 3, the flux calibration is described in Sect. 4 and the data processing is given in Sect. 5.

## 2. Observations

The Nançay radiotelescope (France) is a single dish antenna with a collecting area of 6912 $m^2$ (200 × 34.56) equivalent to that of a 94 m-diameter parabolic dish. The half-power beam width at 21-cm is 3.6 arcmin (EW) × 22 arcmin (NS) (at zero declination). The minimal system temperature at $\delta$ = 15° is about 35 K in both horizontal and vertical polarizations. The spectrometer is a 8192-channel autocorrelator offering a maximal bandwidth of 50 MHz. In this mode, and with two banks in vertical and horizontal polarizations counting 4096 channels each, the spacing of the channels corresponds to 2.6 $km\,s^{-1}$ at 21 cm. After boxcar smoothing the final resolution is typically ∼10 $km\,s^{-1}$. The 50 MHz bandwidth is centered on ∼1387 MHz, thus corresponding to an interval of 10 500 $km\,s^{-1}$ centered on a velocity of 7000 $km\,s^{-1}$ (except for the few objects with a radial velocity known to be less than 2000 $km\,s^{-1}$, for which the observing band was centered on 5000 $km\,s^{-1}$). The gain of the antenna has been calibrated according to Fouqué et al. (1990); the final HI-fluxes (Table 1) are calibrated using as templates a set of well-defined radio continuum sources observed each month. Since the exposure time of an object is often spread over several weeks or months, the total integration is also controlled afterwards by using a set of 58 calibrator galaxies observed over a shorter time scale (see Sect. 5.3).

We used the Nançay processing packages NAPS (NAnçay Preprocessing Software) and SIR (Système Interactif de Réduction). The former allows us to reduce, calibrate, integrate and clean the series of elementary spectra acquired during one meridian transit. The latter allows us to integrate several meridian transit spectra, to produce the final reduced spectrum, and to extract the useful astrophysical parameters. One "observation" is a series of ON/OFF observational sequences; each sequence is made of ten elementary integrations of 4 s each, plus a set of 3 integrations of 2 s for the calibration, adding up in each cycle to 40 + 6 s for the source and 40 + 6 s for the comparison field (hereafter cf). The cf is taken at exactly the same positions of the focal track as the source in the same cycle. In this way one minimizes efficiently the difference between ON and OFF total power. A typical meridian transit observation lasts about 35 min and is centered on the meridian, where the gain is known to be at its maximum; it contains a series of ∼20 ON/OFF cycles.

**Table 2.** Astrophysical HI-parameters (excerpt). Column 1: PGC or LEDA galaxy name; Col. 2: most usual galaxy name; Col. 3: J2000 equatorial coordinates; Col. 4: systemic heliocentric radial velocity (km s$^{-1}$); Col. 5: rms error (km s$^{-1}$); Col. 6: total line width at 20% of the maximum intensity (km s$^{-1}$); Col. 7: total corrected line width at 20% (km s$^{-1}$); Col. 8: rms error (km s$^{-1}$); Col. 9: total line width at 50% of the maximum intensity (km s$^{-1}$); Col. 10: total corrected line width at 50% (km s$^{-1}$); Col. 11: rms error (km s$^{-1}$); Col. 12: observed HI-flux (Jy km s$^{-1}$); Col. 13: beam-filling corrected HI-flux (Jy km s$^{-1}$); Col. 14: rms error (Jy km s$^{-1}$); Col. 15: signal to noise ratio; Col. 16: quality code (see Sect. 4) Col. 17: flag ("*" marks a second independent measurement of lower quality, the 21-cm profile is not plotted in Fig. 4).

| pgc/leda | Name | RA (2000) Dec | $V_{20}$ | $\sigma_V$ | $W_{20}$ | $W_{20c}$ | $\sigma_{W20}$ | $W_{50}$ | $W_{50c}$ | $\sigma_{W50}$ | $F$(HI) | $F$(HI)$_c$ | $\sigma_F$ | $S/N$ | $Q$ | dble |
|---|---|---|---|---|---|---|---|---|---|---|---|---|---|---|---|---|
| pgc0000040 | PGC 000040 | J000035.6-014549 | 7274. | 10. | 314. | 307. | 30. | 288. | 286. | 20. | 4.91 | 4.98 | 1.10 | 5.2 | B | |
| pgc0000068 | ESO 538-017 | J000055.3-185733 | 7679. | 21. | 269. | 262. | 62. | 215. | 213. | 41. | 1.53 | 1.54 | 0.49 | 3.6 | B | |
| pgc0000287 | NGC 7813 | J000409.2-115904 | 9096. | 13. | 391. | 384. | 39. | 376. | 374. | 26. | 4.92 | 4.98 | 1.41 | 3.0 | B | |
| pgc0000312 | PGC 000312 | J000505.3-070537 | 3807. | 3. | 331. | 324. | 8. | 310. | 308. | 5. | 16.48 | 16.99 | 0.99 | 17.7 | A | |
| pgc0000325 | PGC 000325 | J000445.8-160151 | 10092. | 19. | 293. | 286. | 57. | 204. | 202. | 38. | 4.77 | 4.92 | 1.21 | 5.0 | B | |
| pgc0000367 | NGC 7821 | J000516.5-162835 | 7412. | 10. | 536. | 529. | 29. | 525. | 523. | 20. | 4.85 | 4.88 | 1.07 | 3.4 | C | |
| pgc0000483 | NGC 7828 | J000626.9-132454 | 5729. | 15. | 404. | 397. | 46. | 342. | 340. | 30. | 4.14 | 4.27 | 0.76 | 5.2 | C | |
| pgc0000637 | PGC 000637 | J000835.8-051301 | – | – | – | – | – | – | – | – | – | – | – | – | E | |
| pgc0000743 | PGC 000743 | J001036.7-063824 | 8166. | 13. | 311. | 304. | 38. | 294. | 292. | 25. | 3.21 | 3.25 | 1.03 | 3.3 | B | |
| pgc0000817 | ESO 409-026 | J001146.9-300804 | 7788. | 19. | 370. | 363. | 57. | 326. | 324. | 38. | 5.86 | 5.99 | 1.71 | 3.5 | B | |
| pgc0000902 | PGC 000902 | J001334.3-050534 | 5404. | 11. | 332. | 325. | 34. | 306. | 304. | 23. | 4.09 | 4.19 | 0.92 | 4.5 | A | |
| pgc0000902 | PGC 000902 | J001334.3-050534 | 5398. | 9. | 392. | 385. | 26. | 371. | 369. | 17. | 5.06 | 5.18 | 0.91 | 5.4 | A | * |
| pgc0000916 | PGC 000916 | J001347.8-042831 | 11189. | 29. | 454. | 447. | 86. | 425. | 423. | 57. | 1.12 | 1.15 | 0.57 | 1.9 | E | |
| pgc0001012 | PGC 001012 | J001506.8-240542 | 7705. | 25. | 396. | 389. | 75. | 363. | 361. | 50. | 3.87 | 3.90 | 1.60 | 2.3 | C | |
| pgc0001022 | PGC 001022 | J001517.3-062044 | 7781. | 12. | 339. | 332. | 36. | 319. | 317. | 24. | 2.55 | 2.60 | 0.69 | 3.8 | B | |
| pgc0001085 | NGC 0061B | J001624.4-061922 | 8152. | 20. | 362. | 355. | 61. | 360. | 358. | 41. | 0.36 | 0.37 | 0.62 | 0.7 | E | |
| pgc0001149 | NGC 0064 | J001730.4-064930 | 7309. | 10. | 422. | 415. | 29. | 402. | 400. | 20. | 5.64 | 5.78 | 1.13 | 4.6 | B | |
| pgc0001152 | PGC001152 | J001736.3-043735 | 6007. | 10. | 261. | 254. | 31. | 223. | 221. | 20. | 3.64 | 3.68 | 0.69 | 6.1 | B | |
| pgc0001173 | ESO 350-007 | J001804.6-335229 | 7383. | 26. | 604. | 597. | 77. | 593. | 591. | 51. | 8.09 | 8.30 | 4.63 | 1.3 | D | |
| pgc0001206 | PGC 001206 | J001836.1-061805 | 6422. | 5. | 287. | 280. | 15. | 268. | 266. | 10. | 6.24 | 6.26 | 0.80 | 8.6 | A | |
| pgc0001234 | IC 0008 | J001902.4-031322 | 6002. | 10. | 552. | 545. | 31. | 525. | 523. | 21. | 4.52 | 4.56 | 0.81 | 5.0 | C | |
| pgc0001288 | PGC 001288 | J002000.1-062002 | 3707. | 9. | 302. | 295. | 28. | 288. | 286. | 19. | 2.10 | 2.13 | 0.70 | 4.0 | C | |
| pgc0001299 | IC 0012 | J002015.1-023908 | 6044. | 11. | 374. | 367. | 34. | 356. | 354. | 22. | 3.81 | 3.82 | 0.93 | 3.8 | B | |
| pgc0001404 | PGC 001404 | J002151.1-092932 | 6269. | 7. | 333. | 326. | 21. | 321. | 319. | 14. | 3.17 | 3.18 | 0.73 | 4.9 | B | |
| pgc0001453 | PGC 001453 | J002238.1-240733 | 9911. | 29. | 271. | 264. | 88. | 252. | 250. | 58. | 1.86 | 1.86 | 1.69 | 1.5 | D | |
| pgc0001566 | UGC 00237 | J002459.8+063953 | – | – | – | – | – | – | – | – | – | – | – | – | E | |
| pgc0001606 | NGC 0107 | J002542.1-081658 | 6289. | 10. | 282. | 275. | 31. | 208. | 206. | 20. | 5.92 | 5.96 | 0.88 | 8.5 | C | |
| pgc0001693 | NGC 0120 | J002730.1-013048 | 3984. | 12. | 524. | 517. | 37. | 505. | 503. | 24. | 4.49 | 4.70 | 1.08 | 3.6 | C | |
| pgc0001759 | IC 0018 | J002835.1-113509 | – | – | – | – | – | – | – | – | – | – | – | – | E | |
| pgc0001833 | ESO 410-013 | J002955.7-272948 | 7331. | 11. | 348. | 341. | 32. | 304. | 302. | 22. | 4.66 | 4.76 | 0.84 | 6.2 | B | |
| pgc0001886 | PGC 001886 | J003058.8-071258 | 7817. | 8. | 399. | 392. | 24. | 387. | 385. | 16. | 4.48 | 4.52 | 1.04 | 4.4 | B | |
| pgc0001995 | PGC 001995 | J003320.5-095408 | 10566. | 5. | 340. | 333. | 16. | 328. | 326. | 11. | 3.38 | 3.42 | 0.53 | 6.6 | A | |
| pgc0002086 | PGC 002086 | J003502.9-092208 | 6872. | 15. | 342. | 335. | 44. | 308. | 306. | 29. | 2.91 | 2.96 | 0.72 | 4.0 | B | |
| ... | ... | ... | ... | ... | ... | ... | ... | ... | ... | ... | ... | ... | ... | ... | ... | |

The processing chain consists of selecting good elementary integrations or cycles, masking and interpolating areas in the time-frequency plane, straightening the base-line by a polynomial fit, and applying a boxcar smoothing. The maximum of the line profile is determined by eye as the mean value of the maxima of its two horns after taking into account the medium noise (estimated in the base-line). The widths, measured at the standard levels of 20% and 50% of that maximum, correspond to the "distance" separating the two external points of the profile at these intensity levels.

The total list of corrected HI-astrophysical parameters (Table 2), 21-cm line profiles (Fig. 4), and comments

**Table 3.** Notes on HI-observations (excerpt). Column 1: PGC or LEDA galaxy name; Col. 2: morphological type as known in HYPERLEDA; Col. 3: isophotal diameter $D_{25}$ in arcmin; Col. 4: position angle counted from the North (pa = 0) toward East between 0 and 180; Col. 5: quality code (see Sect. 2); Col. 6: comments; conf = "HI confusion", comp = "companion", cf = "comparison field", poss = "possible", w = "with".

| pgc/leda | Morph. | $D_{25}$ (arcmin) | pa (deg) | $Q$ | Comments |
|---|---|---|---|---|---|
| pgc0000040 | | 0.79 | 125 | B | |
| pgc0000068 | Sc | 0.77 | 10 | B | Possibly dbl, comp. not seen in DSS |
| pgc0000287 | Sb | 0.78 | 158 | B | Low velocity edge not well defined |
| pgc0000312 | Sb | 2.28 | 75 | A | |
| pgc0000325 | SBc | 1.36 | 100 | B | |
| pgc0000367 | Sc | 1.17 | 111 | C | Disturbed profile, prob dble w p3093868 |
| pgc0000483 | Scd | 1.38 | 140 | C | Close comp p488 (n7829) at $V$ = 5694, interacting gal.(?) |
| pgc0000637 | Sa | 1.10 | 155 | E | Behind interference at $V$ = 11 500 |
| pgc0000743 | Sbc | 0.90 | 42 | B | |
| pgc0000817 | Scd | 1.22 | 125 | B | |
| pgc0000902 | Sb | 1.09 | 170 | A | |
| pgc0000902 | Sb | 1.09 | 170 | A | |
| pgc0000916 | Sa | 0.89 | 145 | E | No detection |
| pgc0001012 | Sb | 0.77 | 110 | C | galaxy group, poss conf w ESO473-004 $V$ = 7644 |
| pgc0001022 | | 0.93 | 76 | B | |
| pgc0001085 | SO | 1.16 | 0 | E | |
| pgc0001149 | SBbc | 1.41 | 30 | B+ | |
| pgc0001152 | Sc | 0.87 | 142 | B | |
| pgc0001173 | SO-a | 1.30 | 90 | D | Too noisy baseline and too few integrations |
| pgc0001206 | Sc | 0.54 | 0 | A | |
| pgc0001234 | Sc | 0.74 | 128 | C | Confused profile, p1228 (E?) at $V$ = 6186, p1076207 also in beam |
| pgc0001288 | Sab | 1.52 | 35 | C | |
| pgc0001299 | Sab | 0.81 | 19 | B | |
| pgc0001404 | Sc | 1.02 | 156 | B | |
| pgc0001453 | | 0.22 | 0 | D | |
| pgc0001566 | SBa | 0.99 | 70 | E | |
| pgc0001606 | Sbc | 0.79 | 25 | C | Poss conf w pgc143534 |
| pgc0001693 | SO | 1.52 | 73 | C | |
| pgc0001759 | SBb | 1.44 | 15 | E | Conf w pgc0001762? |
| pgc0001833 | Sb | 1.04 | 82 | B | |
| pgc0001886 | Sb | 1.11 | 32 | B | |
| pgc0001995 | | 0.89 | 69 | A | |
| pgc0002086 | S? | 0.84 | 35 | B | |
| ... | ... | ... | ... | ... | ... |

concerning the profiles (Table 3), are available in electronic form at the CDS. As an example, the first page of each are presented at the end of this paper.

## 3. Sample characteristics and input catalogue selection

The **KLUN+** sample has been collected and selected on the basis of the whole sky photometrical surveys **DENIS** ($I$, $J$ and $K$ bands, 95% of the southern sky), **DSS** ($B$ band, whole sky), and **2-MASS** ($J$, $H$ and $K$ bands, whole sky). Basically, we chose as a reference the completeness of the DENIS survey in the $I$-band, that is $I$ = 14 mag for a very conservative magnitude limit. From the observed mean color indexes of spiral galaxies, we determined equivalent flux limits in the other bands, giving $J \leq 13.7$, $H \leq 13.0$ and $K \leq 12.7$. We also restricted the sample according to axis ratios ($R = \frac{a_{25}}{b_{25}}$), eliminating both face-on galaxies ($\log R \leq 0.15$) and very edge-on objects ($\log R \geq 0.48$) to avoid the largest relative errors on the maximum of rotation velocity $\log V_{\rm m}$ (deduced from 21-cm line widths), in particular through large uncertainties on inclinations, which are generally calculated from axis

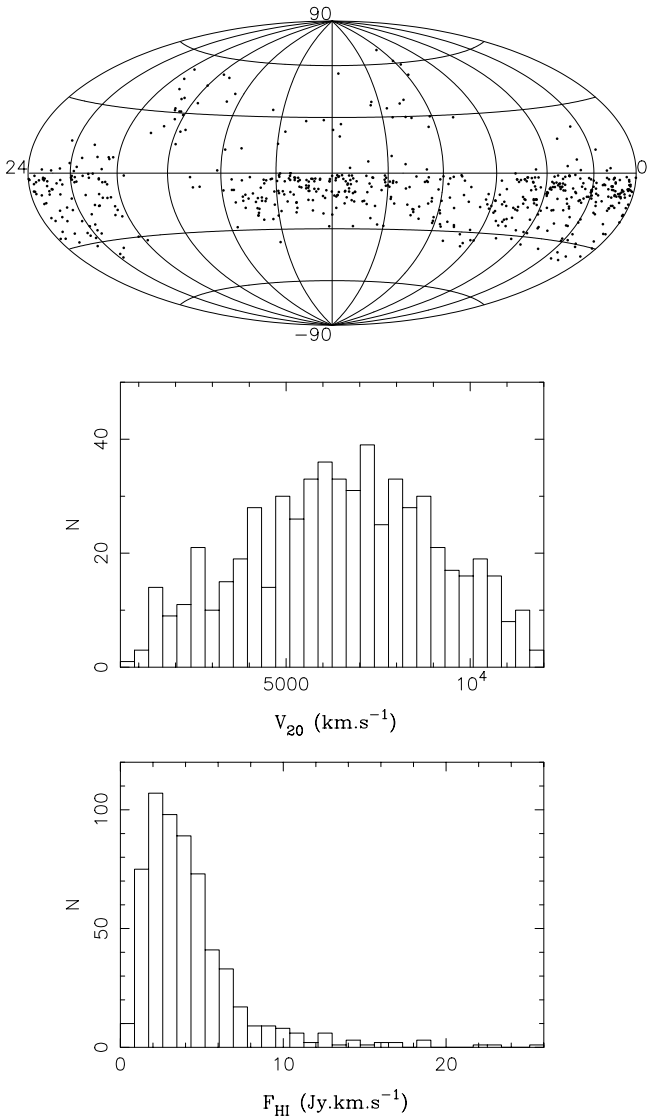


**Fig. 1.** Aitoff projection of the observed sample in J2000 equatorial coordinates, histogram of radial velocities $V_{20}$ and HI fluxes (see Table 2).

ratios and morphological type. The remaining 48 422 selected objects have been inspected by eye on DSS images in order to keep only fair spiral galaxies (this morphological information will be published elsewhere). The HI survey was designed to observe a range of radial velocities of 1800−12 300 km s$^{-1}$ and an extra cut-off in redshift is applied afterwards. Taking into account that the Nançay RT field of view is limited to declinations greater than −40 degrees, thus to 83% of the sky, we are left with a sample of ∼10 000 spiral galaxies among which ∼4100 already have an HI measurement from the literature and our previous programmes.

In the first two years of observations, we have observed 1528 galaxies, detected 870 of them and fully reduced 682 HI profiles. We present here the spectra obtained for 758 of these observed galaxies. The majority of the objects observed are in the range (−30°,+0°) in declination, favouring galaxies having an *I*-band magnitude in DENIS and thus also the declination range unreachable by ARECIBO.

## 4. Flux calibration

The way the calibration is performed is the following: passband filter data are acquired simultaneously with the spectra and are digitalized with a 12-bit converter so that the fluxes are first all expressed in bits (bit$_{\rm fil}$). Each series of 10 integrations (ON or OFF) starts with a calibration phase counting three measurements: one with the noise diode switched off and two with the noise diode on. All are done through the filter. From the former is derived the system temperature ($T_{\rm sys}$), from the average of the two latter, one gets the deviation of the noise diode ΔND. The noise diode deviation in Jy, for a given filter, wavelength and polarization, is controlled and measured regularly using as templates a set of well-defined radio continuum sources. The corresponding data are stored in a calibration table available to all instrument users.

The final spectrum in Jy is given by:

$$\text{spectrum(Jy)} = S_{\,\text{autocor}} \times \frac{T_{\rm sys}(\text{bit}_{\rm fil})}{\Delta\text{ND}(\text{bit}_{\rm fil})} \times \Delta\text{ND(Jy)}$$

$S_{\,\text{autocor}}$ is the normalized spectrum corresponding either to one ON or one OFF elementary integration (the spectrum is normalized by its own total power; in practice it is obtained by Fourier Transform (FFT) using a normalized autocorrelation function), and the term ΔND(Jy) is taken from the instrument calibration table using the closest date of measurement. The advantage of this method is to provide conditions for a robust FFT estimation.

We show in Table 1 the 23 template sources used for the absolute calibration. These sources are point-like and either QSOs or radiogalaxies. Their flux at various wavelength or polarization is directly taken from the cited publication or eventually interpolated from it. In practice, the full set of templates is observed every 3 months over 16 frequencies spread between 1250 MHz and 3349 MHz and over 4 polarizations. One source, 3C123, is observed each month in the above conditions. The fluxes are obtained by drift scans, always within an interval of ±25 m around the meridian. The maximum of intensity is obtained by a Gaussian fit and is compared to the reference table after correcting for the gain curve (as a function of declination, see Fig. 3). Figure 2 shows the mean value of the template's fluxes as a function of time (on the bottom horizontal axis, the number of days after January 31st 2001).

## 5. Data description

Table 2 contains all the reduced HI parameters. Table 3 provides corresponding comments, when necessary, for each galaxy. As in Paturel et al. (2003), we have chosen to classify the spectra and the extracted data according to their quality. We define five classes as follows:

- A: high quality spectrum, high signal to noise and well defined HI profile.
- B: good signal to noise ratio, line border well defined, still suitable for Tully-Fisher applications.
- C: low signal to noise, noisy or asymmetrical profile, well detected but one should not trust the line width. The radial velocity is perfectly determined.

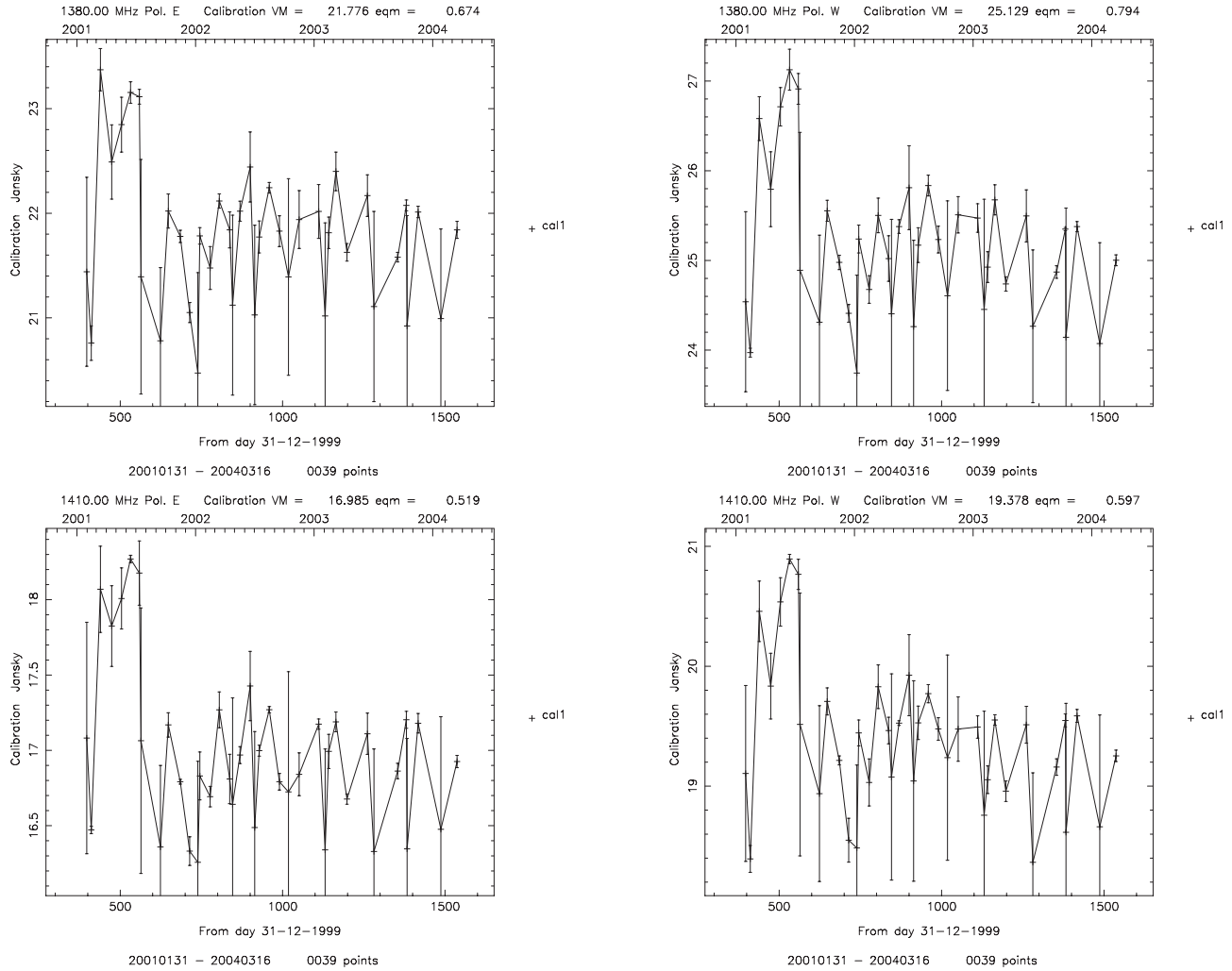


**Fig. 2.** Summary of template radiosource flux measurement in period 2001−2002. The four panels show the mean value of the observed fluxes for the 23 templates as a function of date for two frequencies (1380 MHz and 1410 MHz) and two polarization (E and W).

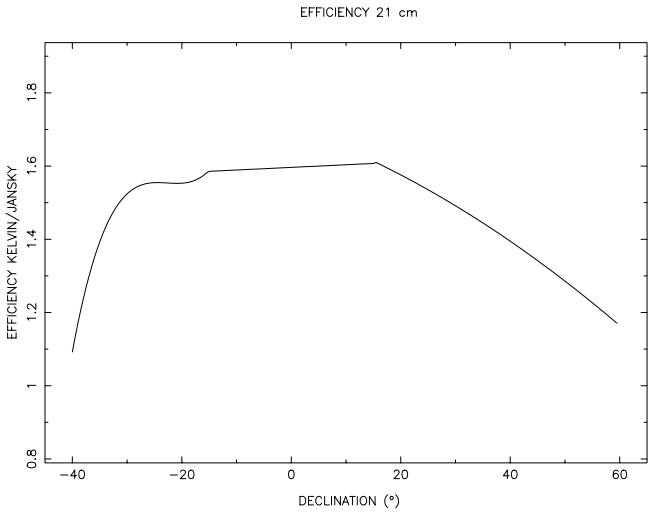


**Fig. 3.** Gain curve of the antenna as a function of declination.

– D: low signal to noise, noisy profile at the limit of detection. Probably detected, but even radial velocity could be doubtful.

– E: not detected. When "no detection" is stated, the line was expected to fall within the observed frequency band and the value of the noise gives a fair upper limit for the HI signal.

We present in Table 1 the results of the observations concerning a total of 758 galaxies, among which 586 have been succesfully detected at 21-cm, in the frequency band we were sampling. The absence of detection, corresponding to the "E" code in the notes, is due to several possible reasons: either the object was too faint in HI to be detected within a reasonable integration time (120 full ON/OFF cycles, equivalent to 3 meridian transit), which is probably the major case, or we did not know its radial velocity and it fell outside the frequency range, or the HI line was always behind a radar emission or an interference... Among the detected objects, 46 were assigned to the "D" class, 172 to the "C" class, and respectively 220 and 148 to either the "B" or "A" class. For a few objects, a second independent measurement, taken in another run, is also given (marked with a star in the last column of Table 2). For these we show only the best quality HI profile in Fig. 7.

The Aitoff projection of the catalogue in J2000 equatorial is seen in Fig. 1, together with the distribution of the radial

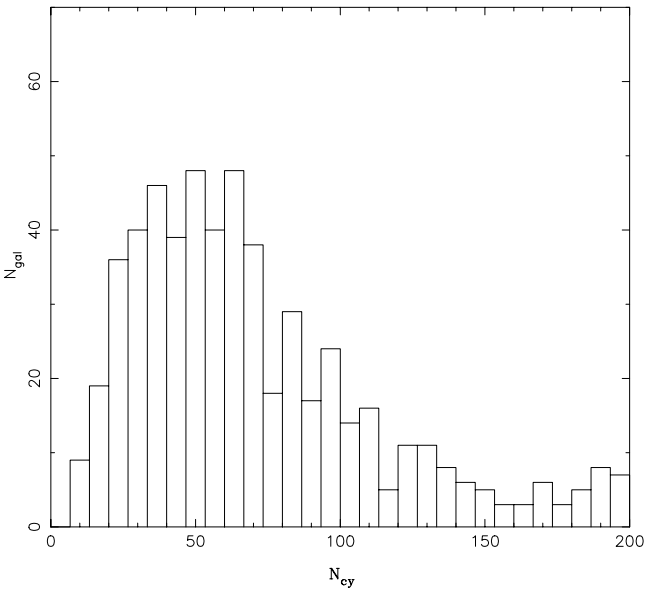


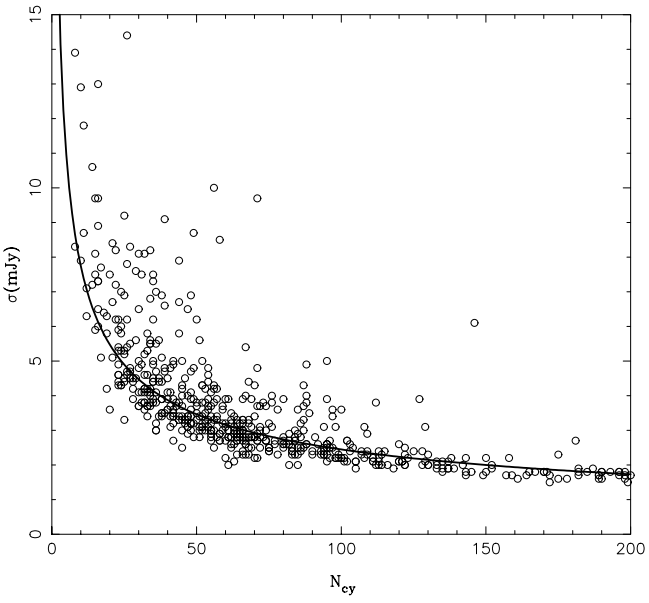


**Fig. 4.** *Upper panel*: distribution of integration time per galaxy in units of ON/OFF cycles number. *Lower panel*: rms noise $\sigma$ in mJy as a function of integration time expressed in number of integration cycles; the solid line is the function $24.5/\sqrt{N_{\rm cy}}$.

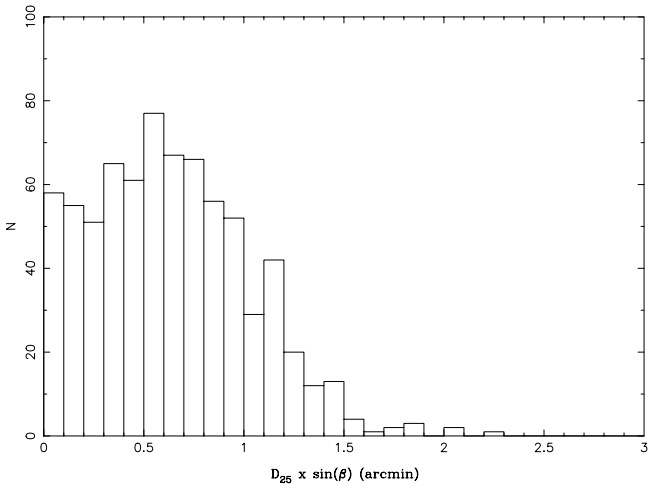


**Fig. 5.** Projection of the major axis $D_{25}$ on the East-West direction.

velocities and HI fluxes. Most of the observed objects are in the range 4000−10 000 km s$^{-1}$ where the lack of Tully-Fisher measurements in the literature is the most critical.

The general statistics of the survey are the following:

- On average, from the allocated time that has been actually used for observing, about one third was lost due to RFI (Radio Frequency Interferences) or receiver problems.
- 41% of final HI spectra have a signal to noise ratio (S/N) greater than 5, while 78% have a SNR greater than 3.
- The upper panel of Fig. 4 shows the histogram of integration time in units of ON/OFF cycles number. Most of the galaxies were measured in less than 75 cycles, equivalent to about 75 min tracking in two polarizations (typically 2.5 meridian transits).
- The lower panel of the same figure shows the rms noise in mJy against the integration time. We reach a 2 mJy rms in 150 cycles, thus in 2.5 h of tracking, while 3.2 mJy is reached in one hour (observing ±15 min around the meridian).

### 5.1. Radial velocities

Our observed radial velocities are listed in Table 2 (Col. 4) and correspond to the median point of the 21-cm line profile measured at 20% of maximum intensity.

The internal mean error on $V_{20}$ is calculated according to Fouqué et al. (1990) as follows:

$$\sigma(V_{20}) = \frac{4 \cdot (R \cdot \alpha)^{1/2}}{S/N}$$

where $R$ is the actual spectral resolution, $\alpha = (W_{20} - W_{50})/2$ is the slope of the line profile, and $S/N$ is the signal to noise ratio. The average of $\sigma(V_{20})$ is about 8 km s$^{-1}$.

### 5.2. Line widths

Line widths are measured on the observed profile at two standard levels corresponding to 20% and 50% of the maximum intensity of the line. The results listed in Table 2, Cols. 6 and 9, have been corrected to the optical velocity scale. We also provide line widths corrected for resolution effect (Fouqué et al. 1990) in Cols. 7 and 10. The mean measurement error is taken equal to $3 \cdot \sigma(V_{20})$ and $2 \cdot \sigma(V_{20})$ for the 20% and 50% widths, respectively. The data presented here are not corrected for internal velocity dispersion. Details about these corrections can be found in Bottinelli et al. (1990), Fouqué et al. (1990) or in Paturel et al. (2003).

**Table 4.** Template galaxies: Col. 1: PGC or HYPERLEDA galaxy name; Col. 2: right ascension (2000); Col. 3: declination (2000); Col. 4: morphological type; Col. 5: $\log D_{25}$ isophotal diameter; Col. 6: $\log R_{25}$ axis ratio; Col. 7: total $B$ magnitude; Col. 8: total line width at 20% of the maximum intensity (km s$^{-1}$) (HYPERLEDA); Col. 9: 21-cm magnitude (HYPERLEDA); Col. 10: HI-flux in Jy km s$^{-1}$; (Theureau et al. 1998); Col. 11: systemic heliocentric radial velocity (km s$^{-1}$) (Theureau et al. 1998).

| pgc/leda | RA (2000) Dec | type | $\log D$ | $\log R$ | $B_t$ (mag) | $W_{20}$ (km s$^{-1}$) | $m_{21}$ (mag) | $F_0$ (Jy km s$^{-1}$) | $V_h$ (km s$^{-1}$) |
|---|---|---|---|---|---|---|---|---|---|
| pgc0000878 | 00 13 03 14 24 32 | Sc | 0.97 | 0.27 | 14.8 | 128.8 | 15.37 | 6.2 | 2026. |
| pgc0001715 | 00 27 52 –1 48 37 | Sc | 1.12 | 0.24 | 14.0 | 265.5 | 14.62 | 8.0 | 4059. |
| pgc0001909 | 00 31 13 –10 28 58 | Sbc | 1.05 | 0.17 | 14.3 | 307.0 | 14.72 | 11.7 | 3588. |
| pgc0002138 | 00 35 40 –20 07 35 | Sb | 1.31 | 0.39 | 13.7 | 331.5 | 14.11 | 20.8 | 3295. |
| pgc0002806 | 00 47 54 19 35 48 | Sc | 1.35 | 0.16 | 14.1 | 361.0 | 14.54 | 11.5 | 4560. |
| pgc0009355 | 02 27 34 41 58 39 | Sb | 0.92 | 0.17 | 14.4 | 279.5 | 14.66 | 12.5 | 5652. |
| pgc0009800 | 02 34 24 –10 50 38 | Sbc | 1.38 | 0.41 | 14.0 | 390.5 | 14.22 | 15.2 | 4767. |
| pgc0010029 | 02 38 51 27 50 51 | Sb | 1.21 | 0.39 | 14.5 | 335.5 | 15.25 | 7.3 | 4578. |
| pgc0010324 | 02 43 36 –16 17 48 | Sab | 1.20 | 0.22 | 15.1 | 311.5 | 15.41 | 6.3 | 7663. |
| pgc0010669 | 02 49 07 –16 59 34 | Sc | 1.28 | 0.40 | 13.1 | 371.5 | 15.00 | 7.8 | 3465. |
| pgc0013194 | 03 33 51 –21 27 17 | Scd | 1.12 | 0.16 | 15.1 | 171.5 | 15.31 | 6.9 | 4063. |
| pgc0019512 | 06 44 00 12 24 10 | Sbc | 1.14 | 0.44 | 14.9 | 425.5 | 15.23 | 6.6 | 3941. |
| pgc0019549 | 06 45 41 22 25 45 | Sbc | 0.98 | 0.40 | 16.5 | 233.5 | 15.50 | 5.8 | 4466. |
| pgc0020256 | 07 09 10 28 41 43 | Scd | 0.89 | 0.18 | 16.7 | 82.5 | 16.25 | 2.9 | 4980. |
| pgc0021161 | 07 30 18 –31 35 54 | Sb | 1.22 | 0.32 | 14.2 | 298.4 | 13.80 | 19.4 | 2087. |
| pgc0021687 | 07 44 34 –13 06 48 | Sc | 1.19 | 0.19 | 0.0 | 126.5 | 14.39 | 16.0 | 2306. |
| pgc0023723 | 08 27 34 –12 45 23 | Sc | 1.37 | 0.21 | 13.2 | 221.5 | 14.92 | 9.9 | 2801. |
| pgc0025221 | 08 58 46 –3 42 38 | Sbc | 1.29 | 0.24 | 13.5 | 253.5 | 14.99 | 7.1 | 2760. |
| pgc0025231 | 08 58 56 –4 54 04 | Sbc | 1.33 | 0.15 | 13.0 | 344.2 | 14.16 | 15.4 | 3714. |
| pgc0027045 | 09 31 36 –30 18 28 | Sc | 1.10 | 0.46 | 14.3 | 242.5 | 14.77 | 11.3 | 2577. |
| pgc0027810 | 09 43 17 –9 56 44 | Scd | 1.36 | 0.34 | 13.9 | 322.5 | 14.56 | 17.0 | 2699. |
| pgc0028366 | 09 51 06 9 00 29 | Sc | 1.30 | 0.17 | 14.0 | 319.5 | 15.08 | 8.2 | 5198. |
| pgc0028376 | 09 51 15 –32 45 17 | Sb | 1.42 | 0.25 | 12.4 | 403.4 | 14.40 | 13.0 | 2785. |
| pgc0029298 | 10 05 39 –37 05 15 | Sc | 1.07 | 0.41 | 14.6 | 337.5 | 15.61 | 5.2 | 4808. |
| pgc0031493 | 10 36 52 –32 20 53 | Sab | 1.38 | 0.48 | 13.5 | 385.1 | 14.37 | 9.7 | 2861. |
| pgc0031653 | 10 38 50 –11 38 54 | Sc | 1.40 | 0.31 | 13.7 | 274.9 | 14.09 | 18.0 | 2488. |
| pgc0035123 | 11 25 30 63 26 45 | Sbc | 1.27 | 0.17 | 13.2 | 499.5 | 16.01 | 5.5 | 3480. |
| pgc0035669 | 11 33 15 24 26 49 | Sb | 1.25 | 0.21 | 14.8 | 424.5 | 16.18 | 12.5 | 6974. |
| pgc0038250 | 12 04 59 58 06 24 | Sbc | 1.04 | 0.18 | 15.5 | 114.5 | 15.01 | 9.1 | 2605. |
| pgc0038667 | 12 09 46 25 01 34 | Sc | 1.01 | 0.35 | 14.6 | 219.5 | 15.13 | 8.1 | 2573. |
| pgc0038799 | 12 11 07 –31 07 35 | Sab | 1.28 | 0.37 | 13.6 | 195.5 | 14.46 | 15.0 | 2119. |
| pgc0044761 | 13 00 26 –15 17 00 | Sab | 1.36 | 0.40 | 13.1 | 637.5 | 14.39 | 16.0 | 4925. |
| pgc0046321 | 13 17 58 4 24 12 | Sb | 1.21 | 0.31 | 14.8 | 454.5 | 15.87 | 4.1 | 6244. |
| pgc0050784 | 14 13 16 27 00 30 | Sb | 1.25 | 0.28 | 14.5 | 376.8 | 14.66 | 11.1 | 5307. |
| pgc0051471 | 14 24 42 –3 12 44 | Sa | 1.27 | 0.27 | 13.5 | 328.5 | 14.11 | 12.3 | 2747. |
| pgc0051851 | 14 30 43 –27 27 16 | Sbc | 1.10 | 0.15 | 14.2 | 216.5 | 15.39 | 6.4 | 4383. |
| pgc0051890 | 14 31 22 –28 45 00 | Sbc | 1.24 | 0.41 | 13.7 | 552.5 | 14.71 | 12.0 | 6572. |
| pgc0051900 | 14 31 29 –22 22 01 | Sbc | 1.04 | 0.22 | 14.5 | 292.5 | 15.52 | 5.7 | 7164. |
| pgc0052811 | 14 47 25 –13 42 57 | Sb | 1.33 | 0.47 | 13.4 | 402.5 | 14.95 | 9.6 | 2908. |
| pgc0054393 | 15 14 15 20 28 42 | Sb | 1.08 | 0.29 | 15.0 | 319.5 | 15.23 | 7.2 | 4681. |
| pgc0054754 | 15 20 45 –18 20 57 | Sc | 1.11 | 0.38 | 15.1 | 227.5 | 14.87 | 10.3 | 2211. |
| pgc0056023 | 15 46 58 17 53 04 | Sc | 1.21 | 0.27 | 13.4 | 184.8 | 14.42 | 14.9 | 3301. |
| pgc0057205 | 16 07 13 7 58 45 | Sc | 1.23 | 0.29 | 14.2 | 283.5 | 15.25 | 6.8 | 2847. |
| pgc0057891 | 16 21 01 –36 08 31 | Sbc | 1.01 | 0.47 | 15.6 | 426.5 | 13.97 | 23.7 | 4448. |
| pgc0058336 | 16 29 27 21 20 12 | Sc | 1.22 | 0.46 | 15.9 | 242.5 | 14.50 | 15.5 | 2988. |
| pgc0061165 | 17 57 14 12 10 45 | Sc | 1.29 | 0.37 | 13.3 | 306.5 | 14.76 | 12.5 | 2867. |
| pgc0061836 | 18 24 19 71 36 06 | Sbc | 1.16 | 0.30 | 14.5 | 407.5 | 14.80 | 9.0 | 5768. |
| pgc0062338 | 18 44 15 24 08 32 | Sab | 1.29 | 0.29 | 14.6 | 405.3 | 14.69 | 12.2 | 3831. |
| pgc0062380 | 18 46 17 22 36 55 | Sc | 1.10 | 0.15 | 15.0 | 345.5 | 14.98 | 9.3 | 4698. |
| pgc0062548 | 18 54 23 24 39 08 | Sc | 1.11 | 0.34 | 15.4 | 319.5 | 15.06 | 8.7 | 4319. |
| pgc0062781 | 19 07 03 29 00 24 | Sbc | 1.34 | 0.22 | 13.6 | 415.7 | 15.32 | 9.9 | 3912. |
| pgc0063711 | 19 49 35 –26 25 55 | Sbc | 1.34 | 0.18 | 14.1 | 410.5 | 14.95 | 9.6 | 5960. |
| pgc0064458 | 20 18 37 0 09 02 | Sc | 1.32 | 0.48 | 14.4 | 524.3 | 13.93 | 15.8 | 5410. |
| pgc0067373 | 21 48 04 –36 46 19 | Sc | 1.13 | 0.41 | 15.1 | 189.5 | 15.19 | 7.7 | 2547. |
| pgc0067347 | 21 47 16 72 28 18 | Sc | 1.09 | 0.15 | 15.4 | 304.9 | 13.75 | 22.0 | 2403. |
| pgc0068861 | 22 26 11 –31 08 49 | Sb | 1.15 | 0.37 | 14.2 | 278.5 | 14.54 | 14.0 | 4001. |
| pgc0069132 | 22 33 16 –27 14 47 | Sb | 1.22 | 0.35 | 13.7 | 337.3 | 14.58 | 14.8 | 3544. |
| pgc0071430 | 23 26 20 –17 57 24 | Sa | 1.09 | 0.23 | 14.2 | 215.5 | 14.92 | 9.9 | 2873. |

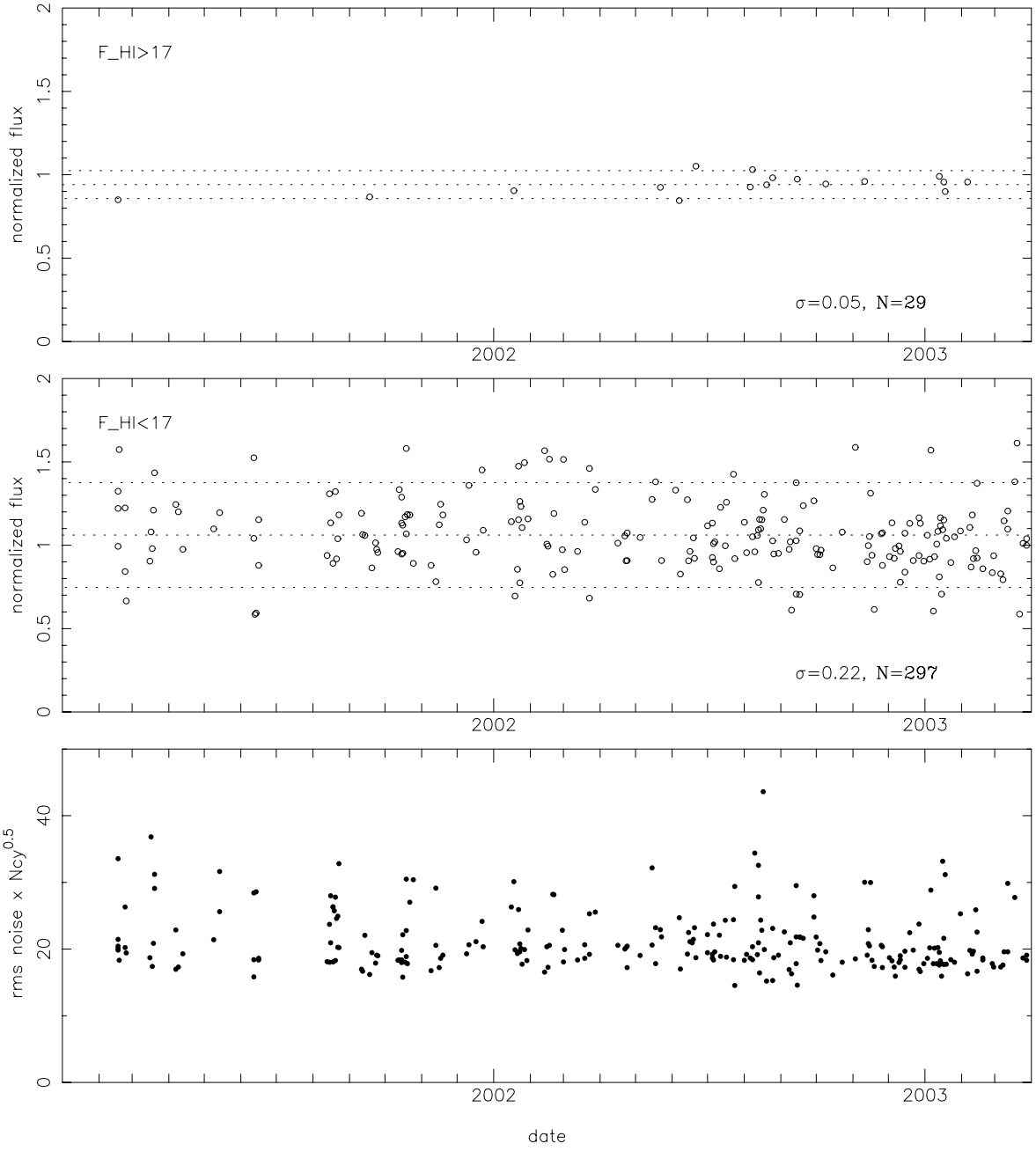


**Fig. 6.** Evolution of the normalized HI-flux ($F_{\rm HI}/F_0$) and rms noise in the baseline for our 58 template galaxies during the survey: **a)** template galaxies with $F_{\rm HI} > 17$ Jy km s$^{-1}$, the dashed lines shows the 1.5$\sigma$ levels, **b)** template galaxies with $F_{\rm HI} < 17$ Jy km s$^{-1}$, **c)** rms noise $\times \sqrt{N_{\rm cy}}$, i.e. rms noise for one single cycle of ON/OFF integration, for all template galaxy measurements.

### 5.3. HI-fluxes

HI-fluxes $F_{\rm HI}$ (Table 2, Col. 12) are expressed in Jy km s$^{-1}$. The values given in Col. 13 are corrected for beam-filling according to Paturel et al. (2003):

$F_{\rm HIc} = B_f \cdot F_{\rm HI}$

where $F_{\rm HI}$ is the observed raw HI-flux,

$B_f = \sqrt{(1 + xT)(1 + xt)}$

$T = \left(a_{25}^2 \sin^2\beta + b_{25}^2 \cos^2\beta\right)/\theta_{EW}^2$

$t = \left(a_{25}^2 \cos^2\beta + b_{25}^2 \sin^2\beta\right)/\theta_{\rm NS}^2$

$\theta_{EW}$ and $\theta_{\rm NS}$ are the half-power beam dimensions of the Nançay antenna, $\beta$ is the position angle of the galaxy defined north-eastwards, $a_{25}$ and $b_{25}$ are the photometric major and minor axis respectively. The parameter $x$ is $x = 0.72 \pm 0.06$ (Bottinelli et al. 1990). The distribution of the East-West projection of $D_{25}$ diameters is shown in Fig. 5. This is to be compared to the 4 arcmin width of the half-power beam.

The total exposure time of a target is often spread over several weeks or months. The flux integration is controlled afterwards according to a set of 58 HI-template galaxies regularly observed during the period covered by our programme. These HI-template galaxies are used exclusively to control the gain

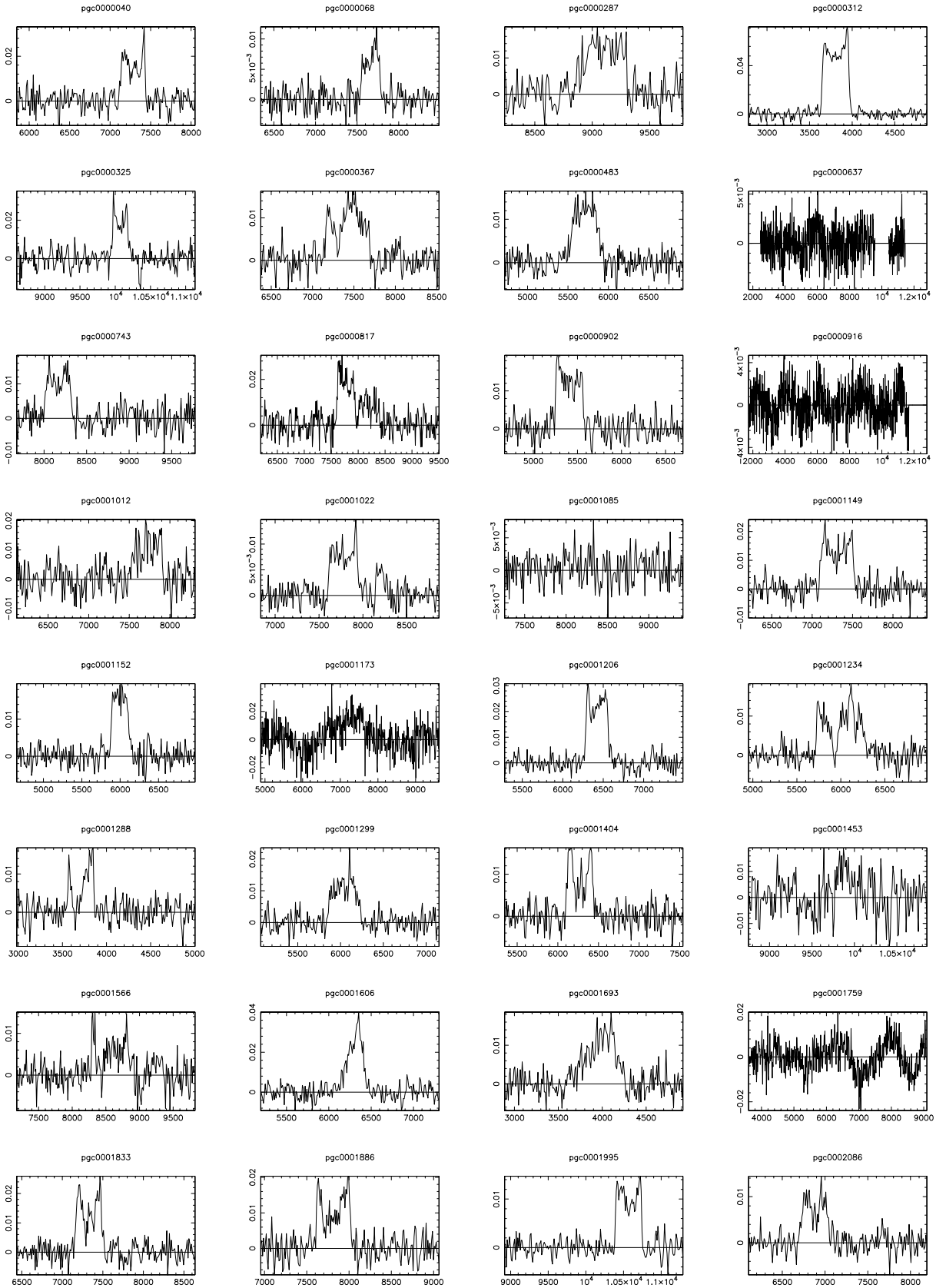


**Fig. 7.** -excerpt. 21-cm line profiles of galaxies listed in Table 2; profiles are classified according to their PGC name appearing in the top right corner of each panel. The usual name of the galaxy (NGC, UGC, IC, ESO, MCG...) is written above each panel. Ordinate and abscissae axes are graduated respectively in km s$^{-1}$ and mJy. Note that heliocentric radial velocities are expressed in terms of optical redshift $c\frac{\Delta\lambda}{\lambda}$. The horizontal line represents the baseline of the profile, from which the maximum is estimated.

stability over short time scales, allowing us to verify that the gain factor has not changed from one meridian transit of the scientific target to another. They were chosen to be as representative as possible of the survey galaxies, covering a wide range of radial velocities and HI fluxes. They have also the great advantage of being distributed over the whole sky, in particular at all right ascensions, providing a large flexibility in observation scheduling, and to be measurable in HI within a 10 min meridian transit... Their HI-fluxes $F_0$ (see Table 4) were accurately measured with the same instrument by Theureau et al. 1998. Note that here, it is not the absolute flux which is supervised, but the variations of its measurement with time, the calibration itself being done by the above continuum sources (Sect. 4).

The evolution of the normalized HI flux $F_{\rm HI}/F_0$ with time is seen in Fig. 6 (upper two panels) separately for the four templates which had the largest flux (pgc21161, pgc27810, pgc31653 and pgc57891) and for low flux galaxies ($F_{\rm HI} < 17$ Jy km s$^{-1}$). The brightest objects at the 21-cm wavelenghth (first panel) show a very narrow distribution around unity along the whole period, with a dispersion $\sigma = 5\%$. Fainter objects also show a regular and constant distribution with time, but with a much larger $\sigma$ of 22%, which could be understood as the mean actual error on our flux measurements for the whole survey. Note that the template galaxy sample allows us to control the instrument calibration over a wide time scale, showing that it was very stable during the whole period of observation. In the bottom panel of Fig. 6, we show the rms noise measured in the spectrum base-line (outside the line and occasional interferences) multiplied by the square root of time in units of ON/OFF integration cycles. It shows the rms noise normalized to one cycle of integration. It was again very stable around 20 mJy during the entire period, perhaps showing a slight decrease of a few percent since mid 2002.

*Acknowledgements.* We have made use of data from the Lyon-Meudon Extragalactic Database (HYPERLEDA). We would like to acknowledge the scientific and technical staff of the Nançay radiotelescope.

## References

Baars, J., Genzel, R., Pauliny-Toth, I., & Witzel, A. 1977, A&A, 61, 99

Barnes, D. G., Staveley-Smith, L., de Blok, W. J. G., et al. 2001, MNRAS, 322, 486

Bottinelli, L., Gouguenheim, L., Paturel, G., & de Vaucouleurs, G. 1983, A&A, 118, 4

Bottinelli, L., Gouguenheim, L., Fouqué, P., & Paturel, G. 1990, A&AS, 82, 391

Bottinelli, L., Durand, N., Fouque, P., et al. 1992, A&AS, 93, 173

Bottinelli, L., Durand, N., Fouque, P., et al. 1993, A&AS, 102, 57 (Paper II)

Bottinelli, L., Gouguenheim, L., Paturel, G., & Teerikorpi, P. 1995, A&A, 296, 64

Fouqué, P. 1982, Ph.D. Thesis, University of Paris

Fouqué, P., Bottinelli, L., Gouguenheim, L., & Paturel, G. 1990, ApJ, 349, 1

Gardner, F., Whiteoak, J., & Morris, D. 1975, AJPAS, 35, 1

Hudson, M. J., Lucey, J. R., Malecki, J. J., et al. 2004, in Galaxy Evolution: Theory and Observations, ed. V. Avila-Reese, C. Firmani, C. Frenk, & C. Allen, Rev. Mex. AA SC, 17, 177

Jarrett, T.-H., Chester, T., Cutri, R., et al. 2000, AJ, 120, 298

Jones, D. H., et al. 2004, MNRAS, submitted [arXiv:astro-ph/0403501]

Hanski, M. O. 2003, in New Results in Cosmology and the Coherence of the Standard Model, XVth Rencontres de Blois, France, held 15–20 June 2003 [arXiv:astro-ph/0309821]

Kuhr, H., Witzel, A., Pauliny-Toth, I., & Nauber, U. 1981, A&AS, 45, 367

Mamon, G. 2000, Cosmic Flows Workshop, ASP Conf. Ser., ed. S. Courteau, & J. Willick, 201, 103

Mamon, G., Giraud, F., Rassia, E., et al. 2004, in Maps of the Cosmos, International Astron. Union. Symp. No. 216, held 14–17 July, 2003 in Sydney, Australia

di Nella, H., Paturel, G., Walsh, A. J., et al. 1996, A&AS, 118, 311

Paturel, G., Fouqué, P., Bottinelli, L., & Gouguenheim, L. 1989, A&AS, 80, 299

Paturel, G., Bottinelli, L., Fouqué, P., Gouguenheim, L., & Teerikorpi, P. 1990, The Messenger, 62, 8

Paturel, G., Fang, Y., Petit, C., Garnier, R., & Rousseau, J. 2000, A&AS, 146, 19

Paturel, G., Bottinelli, L., Di Nella, H., et al. 1994, A&A, 289, 711

Paturel, G., Theureau, G., Bottinelli, L., et al. 2003, A&A, 412, 57

Theureau, G., Bottinelli, L., Coudreau, N., et al. 1998, A&AS, 130, 333

Veron, M. 1972, A&A, 20, 471

Willick, J. 2000, in Proc. of the XXXVth Rencontres de Moriond: Energy Densities in the Universe (Frontières)

Witzel, A., Véron, P., & Véron, M. 1971, A&A, 11, 171